Clathrin Triskelia Show Evidence of Molecular Flexibility

Matthew L. Ferguson,*† Kondury Prasad,‡ Hacene Boukari,† Dan L. Sackett,† Susan Krueger,§ Eileen M. Lafer,‡ and Ralph Nossal†

*Department of Physics, University of Maryland, College Park, Maryland; †Laboratory of Integrative and Medical Biophysics, Eunice Kennedy Shriver National Institute of Child Health and Human Development, National Institutes of Health, Bethesda, Maryland; ‡Department of Biochemistry, University of Texas Health Science Center, San Antonio, Texas; and §NIST Center for Neutron Research, National Institute of Standards and Technology, Gaithersburg, Maryland

ABSTRACT The clathrin triskelion, which is a three-legged pinwheel-shaped heteropolymer, is a major component in the protein coats of certain post-Golgi and endocytic vesicles. At low pH, or at physiological pH in the presence of assembly proteins, triskelia will self-assemble to form a closed clathrin cage, or "basket". Recent static light scattering and dynamic light scattering studies of triskelia in solution showed that an individual triskelion has an intrinsic pucker similar to, but differing from, that inferred from a high resolution cryoEM structure of a triskelion in a clathrin basket. We extend the earlier solution studies by performing small-angle neutron scattering (SANS) experiments on isolated triskelia, allowing us to examine a higher q range than that probed by static light scattering. Results of the SANS measurements are consistent with the light scattering measurements, but show a shoulder in the scattering function at intermediate q values (0.016 $Å^{-1}$), just beyond the Guinier regime. This feature can be accounted for by Brownian dynamics simulations based on flexible bead-spring models of a triskelion, which generate time-averaged scattering functions. Calculated scattering profiles are in good agreement with the experimental SANS profiles when the persistence length of the assumed semiflexible triskelion is close to that previously estimated from the analysis of electron micrographs.

INTRODUCTION

Clathrin is a eukaryotic protein involved in intracellular trafficking (1,2). It is one of several proteins found in the coats of transport vesicles that bud from the plasma membrane and certain regions of the Golgi apparatus. The involvement of protein coats of various kinds is thought to be a general feature of cellular vesicle formation (3).

The basic subunit of a clathrin coat is a hetero-hexameric complex of polypeptides collectively called a clathrin triskelion. In its simplest form, a triskelion can be represented as a trimer of articulated legs that are bent midway along their lengths. Each leg is composed of a clathrin heavy chain and an associated clathrin light chain. The heavy chains are joined at their C-terminal ends at a common hub, from which the legs spread (see Fig. 1). This extended-leg conformation is readily observed in electron micrographs of completed baskets (1,2). A clathrin heavy chain contains two major structural units, one being an α-solenoid repeat that forms the major part of the 520 Å long triskelion leg. Located at the distal end of the leg, after a flexible linker domain, is the second unit consisting of a seven-bladed β-propeller (or WD40) domain. This is a binding domain for clathrin-associated proteins involved in the clathrin-mediated intracellular trafficking pathway. The entire heavy chain is ~1675-amino-acids long and has a molecular mass of ~192,000 g/mole (Da), while the (variable) light chain has a molecular mass between 25,000 and 35,000 Da, depending on tissue type.

Recently, the structure of clathrin complexes has been determined at sufficiently high resolution that individual triskelions can be resolved within the coat complex. In a recent study, we showed that the inferred structures of basket-associated triskelia, although differing somewhat in detail, are roughly consistent with static and dynamic light scattering measurements performed on dilute solutions of isolated clathrin triskelia (4). These measurements provided values of the radius of gyration, R_g, and hydrodynamic radius, R_H, of the triskelia, which we found to be essentially invariant as the pH of the samples is lowered from pH 7.0 to pH 6.0 ($R_g \approx 22$ nm, $R_H \approx 16$ nm). Since the experimental values of R_g and R_H are somewhat larger than those calculated from the coordinates (5) of a triskelion in a small D_6 basket, we concluded that the average shape of a triskelion in solution is slightly more extended than is a typical triskelion in such a structure (4). Moreover, when the data were compared with results of model calculations (4), we inferred that triskelia have a puckered shape in buffers where they do not noticeably polymerize, as well as in buffers in which basket formation is rapid. In these calculations, a simple bead model of a clathrin triskelion was used in which the leg bend and pucker angles (ϕ and ψ, respectively) are treated as variables (see Fig. 1). Several (ϕ,ψ) pairs were found to yield values of R_g and R_H compatible with the observed quantities.

In principle, scattering of shorter wavelength radiation can provide finer resolution of molecular structure than is obtainable using visible light. We thus undertook a small-angle neutron scattering (SANS) study of isolated triskelia and, as shown below, we are now able to better discriminate certain features of the model. The scattered intensity measured by

Submitted November 28, 2007, and accepted for publication April 9, 2008.

Address reprint requests to Ralph Nossal, Tel.: 301-435-9233; E-mail: nossalr@mail.nih.gov.

Editor: Jill Trewhella.

0006-3495/08/08/1945/11 $2.00

doi: 10.1529/biophysj.107.126342

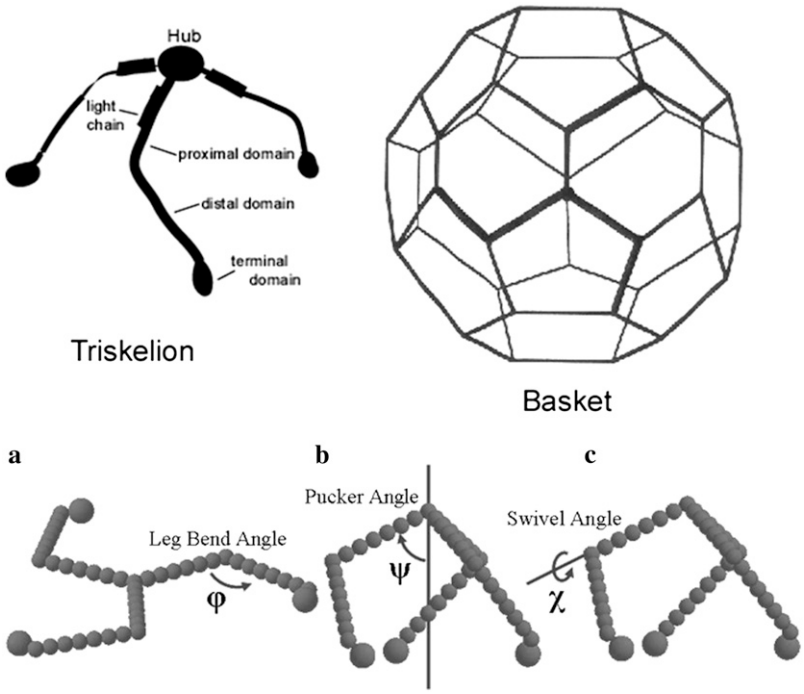

FIGURE 1 Schematic representations of clathrin triskelia. (*Top*) Cartoon showing three clathrin heavy-chain legs joined at a common hub, each heavy chain being associated with a clathrin light chain. Also shown is a sketch of a clathrin basket, indicating how the triskelia form a structure having a buckyball-like appearance. (*Bottom*) Examples of a simple bead model of a clathrin triskelion, defining the leg bend angle, pucker angle, and swivel angle. (*a*) The leg bend angle, ϕ, and (*b*) pucker angle, ψ, were varied from 30° to 180° and 30° to 90°, respectively. (*c*) The swivel angle, χ, was varied parametrically with the pucker angle according to the equation $\chi = 3(\psi-30)/2$, where ψ is measured from the vertical axis shown in panel *b*.

static light scattering (SLS), described in Ferguson et al. 2006 (4), gave the radius of gyration when fit to a Gaussian model function (Guinier approximation; $qR_g \ll 1$): $I(q) \approx e^{-\frac{1}{3}(R_g q)^2}$, where q is the magnitude of the Bragg scattering vector and R_g is the radius of gyration of the triskelion. SANS allowed us to measure the continuation of the scattering cross section beyond the Guinier regime. Since the neutron wavelength is much smaller than that of light (5 Å for neutrons, as opposed to 0.5 μm for light), it was expected that measurements of the scattering cross section at higher resolution would give us more definitive information about triskelial structure than do SLS measurements of R_g. However, due to its large, extended size and unusual shape, the clathrin triskelion differs qualitatively from most other macromolecules that have been analyzed by neutron diffraction. Thus, simple models that frequently are used to interpret SANS measurements would not likely provide good fits to the data. Because the triskelion has a three-armed pinwheel-like tertiary structure, we base our analysis, in part, on information obtained from crystal structures of portions of clathrin heavy chains (6), images of triskelia adsorbed to mica surfaces (7), and structures inferred from assembled clathrin baskets (5,8). (Similarly, in studies of tubulin (9) and actin (10), it has been informative to compare SANS determinations made on proteins in solution with structures measured by x-ray diffraction from crystallized samples and/or electron microscopy.) As described below, in this investigation we utilize SANS and SLS data to infer a model of a triskelion that is consistent over a wide range of q values, using Eq. 1 (see below) as the basis of the analysis.

The angular dependence of the scattered intensity from a randomly oriented molecule of arbitrary shape, approximated as a collection of N identical scatterers, can be calculated by (11)

$$I(q) = N^{-2}\Sigma\Sigma f_i(q) f_j(q) \sin(qr_{ij})/(qr_{ij}), \qquad (1)$$

where the sums are over all particles ($i,j = 1$ to N), $f_i(q)$ is the scattering amplitude of the i^{th} scatterer, r_{ij} the distance between the i^{th} and j^{th} scatterers, and $q = (4\pi n/\lambda)\sin(\theta)$, n being the index of refraction of the sample and 2θ the scattering angle. In early studies, Debye (11) and others evaluated Eq. 1 for molecules of different shapes suspended in solution (12,13). They found, for example,

1. For a uniform and spherical scattering density of radius a:

$$I(q) = \frac{9(\sin(qa) - qa\cos(qa))^2}{q^6 a^6}; \qquad (2)$$

2. For a nonuniform spherical scattering density with a Gaussian radial mass distribution function of width R_g, $\rho(r) = e^{-\frac{r^2}{2R_g^2}}$, corresponding to a random coil (or Gaussian chain):

$$I(q) = \frac{2}{R_g^4 q^4}(e^{-R_g^2 q^2} - (1 - R_g^2 q^2)); \qquad (3)$$

3. For an infinitely thin rigid rod of length L:

$$I(q) = \frac{2}{qL}\int_0^{qL} dx \frac{sinx}{x} - \frac{1}{(qL/2)^2} sin(qL/2)^2. \qquad (4)$$

Cases 1 and 3 are useful for some particles that have well-defined spherical and rodlike shapes, such as some viruses. Case 2 is useful for very flexible objects of any type (commonly studied are different types of linear polymers).

Others have calculated the scattering cross section for a single semiflexible linear chain (14), and found a transition

from q^{-2} behavior to q^{-1} dependence. This transition occurs over a range of q values that is related to the persistence length (a measure of flexibility) of the linear chain, indicating how the scattering cross section of the chain changes as the flexibility varies.

EXPERIMENTAL METHODS

SANS measurements were performed on samples of purified clathrin contained in disassociation buffer (0.5 M Tris + 3 mM dithiothreitol dissolved in H_2O and brought to a pH of 7.0 by the addition of concentrated HCl). Measurements also were made on clathrin in D_2O buffers to reduce incoherent scattering, making it possible to obtain data at higher q values than in an H_2O solvent. There are no notable differences in $I(q)$ over the q range accessible for both samples (see Fig. 2).

Sample preparation

Clathrin triskelia were purified from coated vesicles of bovine brain as described in Morgan et al. (15) and stored in dissociation buffer at 4°C. Before measurement, an aliquot of the sample was centrifuged for 15 min in a tabletop centrifuge at 400,000 × g (where $g = 9.81$ m/s^2). The supernatant, at a final protein concentration of 2.7 mg/mL, was then loaded into a quartz cuvette having a 1-mm pathlength, constituting the clathrin-H_2O sample for our SANS study.

This procedure also was used to prepare clathrin samples in D_2O, except that before centrifugation an aliquot of stock solution was dialyzed into D_2O buffer (see below). The final clathrin concentration of this primary D_2O sample was 1.5 mg/mL and was at a pD* value of 7.0. Reported pD* values were those measured by a glass electrode pH meter, being related to the actual pD($= -log_{10}[D+]$) according to pD = pD* + 0.4 units (16).

D_2O buffers were made by the addition of Tris-HCl to 99.9% D_2O. This dissolved to a pD* of 5.6, allowing us to add NaOH dissolved in D_2O to raise the solution to the desired pD* of 7 without diluting the D_2O. The final buffer contained ≈97% D_2O due to the addition of 3 mL of H_2O and 750 μL of 0.5M dithiothreitol in H_2O to 120 mL of D_2O buffer.

Measurements of protein concentration were made by UV absorbance at a wavelength of 280 nm. The absorption coefficient of ε_{280} was estimated to be 1.07 g^{-1} cm^{-1} from the amino-acid sequence.

Light scattering

Static light scattering (SLS) and dynamic light scattering (DLS) measurements of clathrin in solution were made as described in Ferguson et al. (4). Briefly, for SLS, intensity data were taken every 2°, at scattering angles between 50 and 150°. The logarithm of the intensity profile was plotted against q^2 (where q is the magnitude of the Bragg scattering vector) and fit to a straight line (the Guinier approximation), the slope of which is given as $1/3\,R_g^2$, where R_g is the radius of gyration. In the case of DLS, measurements were made at scattering angles of 90 and 150°, data being collected in the homodyne mode. Photon counts were autocorrelated over a time range from 1 to 10^4 μs, and the method of cumulants was used to obtain an average translational diffusion coefficient, D. The Stokes-Einstein relation then was used to obtain the effective hydrodynamic radius, R_H and equivalent frictional force. Transport properties of presumed clathrin structures were calculated by using HYDRO (a public-domain computer program) to determine how well various models agree with the light scattering data. Details can be found in Ferguson et al. (4).

Neutron scattering

Experiments were performed on the NIST Center for Neutron Research NG-3 30-meter small-angle neutron scattering instrument (17). The wavelength of neutrons used was 5.5 Å ± 0.4 Å (0.8 Å FWHM). Scattered neutrons were detected with a 64 cm × 64 cm two-dimensional position-sensitive detector with 128 × 128 pixels and 0.5 cm resolution per pixel. Sample/detector distances of both 13 meters and 5 meters were used to obtain q values ranging from ≈0.003 Å^{-1} to 0.04 Å^{-1} and 0.01 Å^{-1} to 0.1 Å^{-1}, respectively, where $q = 4\pi\sin(\theta)/\lambda$, λ being the neutron wavelength and 2θ the scattering angle. Multiple data files were recorded over times between 15 min and 1 h and later added together. Total data acquisition times were between 3 and 5 h per sample. Neutron transmission was 83–86% in D_2O and ≈52% in H_2O. Background scattering was measured for empty cuvettes (for 1 h) and buffers in both H_2O (4 h) and D_2O (2 h).

The data were reduced using a commercial program, with SANS macros written at the NCNR (18). Raw counts were normalized to a common monitor count (SAM) and corrected for empty cuvette counts (EMP) and ambient room background counts (BGD), using the relation

$$COR = (SAM - BGD) - [T_{sam}/T_{emp}](EMP - BGD),$$

where T_{sam} and T_{emp} are the transmissions of the sample and empty cuvette, respectively. Adjustments to these background-corrected data were made, on a pixel-by-pixel basis, for nonuniform detector efficiencies, using factors determined from measurements from Plexiglas, which is an isotropic scatterer. The buffers were treated in the same manner as the clathrin + buffer samples at this stage of the data reduction.

Data were placed on an absolute intensity scale in units of cm^{-1}, by normalizing the scattered intensity to the incident beam flux. To find the

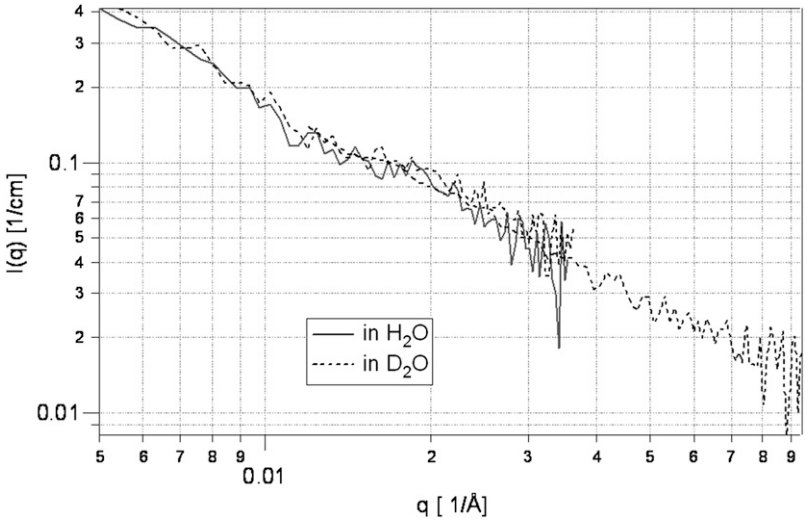

FIGURE 2 SANS data from clathrin in both H_2O (*solid*) and D_2O buffers (*dashed*). (Error bars and symbols have been removed to illustrate the similarity of both curves.) $I(q)$ is given on an absolute scale in units of cm^{-1}. The clathrin concentration of the D_2O sample was 1.5 mg/mL and that of the H_2O sample was 2.7 mg/mL. Because the contrasts are different, were the two samples to be at the same concentration, the D_2O curve would lie above the H_2O curve.

scaling factor, a transmission measurement from an attenuated empty beam was measured under the same experimental conditions (18).

The scattered intensity $I(q)$ is related to the absolute cross section, $d\Sigma/d\Omega$, by the expression

$$I = \phi A \varepsilon d\, T(d\Sigma/\mathrm{d}\Omega)\Delta\Omega t,$$

where ϕ = neutron flux on the sample, A = sample area, ε = detector efficiency, d = sample thickness (1 mm), T = measured sample transmission, $\Delta\Omega$ = solid angle subtended by one pixel of the detector (0.5 cm for this experiment), and t = effective counting time. The quantity $\phi A \Delta\Omega \varepsilon t$ is the scaling factor.

Next, the data were radially averaged to produce curves of scattered intensity, $I(q)$, versus q. The corrected averaged scattered intensities of the appropriate buffers were then subtracted from that of the clathrin + buffer samples. Any remaining flat background scattering was assumed to arise from incoherent scattering from hydrogen in the clathrin itself. If necessary, this remaining flat region was fit to a straight line to determine a constant value that was subtracted from the data.

RESULTS

Testing D_2O as a solvent for clathrin

SANS was first performed on clathrin in H_2O. In those samples our sensitivity was limited to q values for which the scattering intensity due to the presence of protein was on the order of, or larger than, the incoherent scattering due to the solvent. In practice, this limited us to q values <0.025 $Å^{-1}$. Because D_2O has a smaller incoherent scattering cross section than does H_2O (≈ 0.1 cm^{-1} for D_2O versus 1 cm^{-1} for H_2O), higher signal/background can be achieved when D_2O is used as a solvent. However, although D_2O has many of the same physical properties as H_2O, it may affect the structure and behavior of some biological macromolecules (9,19). Therefore, it was important to check that clathrin remains folded properly and maintains its functionality when a D_2O buffer is used as a solvent. In Fig. 2, we show SANS cross sections for 2.7 mg/mL clathrin in H_2O and 1.5 mg/mL clathrin in D_2O, and find that the curves are essentially indistinguishable (see Fig. 2 legend). We also measured several D_2O samples of lower clathrin concentration to establish that there is no noticeable change in $I(q)$ deriving from interactions between triskelia (data not shown).

Clathrin maintains its structure in D_2O

In addition to SANS (see above), light scattering measurements were performed to examine the properties of clathrin in D_2O. We found the index of refraction for D_2O to be very close to that of H_2O (data not shown), which is important because changes in the index of refraction will influence the q dependence and intensity of the scattered light. Another factor to take into account is a possible change in viscosity, which will modify the diffusion of the particles and thereby affect the DLS measurement. Indeed, we found the viscosity to be 22% greater in D_2O as determined by dynamic light scattering from polystyrene spheres of radius ≈ 60 nm, which is consistent with values found in literature (20,21). However, measurements of hydrodynamic radii in both solvents (pH/pD* = 7.0) were comparable once a correction was made in the DLS measurement for the difference in viscosity between the two solvents. (Viscosity-corrected hydrodynamic radii obtained from the light scattering measurements of clathrin in the H_2O and D_2O buffers are $R_H = 15.7$ nm $\pm$ 0.1 nm and $R_H = 15.6$ nm $\pm$ 0.2 nm, respectively.) As mentioned above, corresponding SANS cross sections also are nearly identical.

Neutron scattering and rigid clathrin models

SANS data were compared with theoretical curves of the scattering function, $I(q)$, which were calculated from Eq. 1 for rigid models of clathrin triskelia similar to those used in Ferguson et al. (4). First, a high-resolution model based on the 21 Å and 12.5 Å cryoEM structures of a clathrin triskelion in a D_6 basket (5,8) was investigated by using beads of radius 3.6 Å to represent each amino-acid residue resolved in the structure (22,23), each bead being centered at the coordinates of the C_α atom of a corresponding amino acid. A visualization of the model and the corresponding calculated scattering function can be seen in Fig. 3. In addition, lower resolution, coarse-grained, models consisting of 52 beads were used to estimate the effect of changes in triskelion conformation on the calculated theoretical scattering function. Sixteen beads in any particular leg of these low-resolution models each has a radius of 15 Å, corresponding to $\sim$12 kDa of protein or $\sim$110 amino-acid residues, whereas the terminal domain is modeled by a slightly larger bead having a radius of 25 Å. Visualizations of these models, along with calculated scattering functions, can be seen in Fig. 4. For comparison, in Figs. 3 and 4 we also show experimental SANS data obtained for clathrin triskelia in 0.5 M Tris/D_2O at pD* 7.0. Two characteristic features are observed in the $I(q)$ shown in Figs. 3 and 4 (for the high-resolution and coarse-grained bead models, respectively), that is, a minimum and a secondary maximum at q values just outside of the central Guinier regime. Model calculations (results not shown) indicate that this dip occurs because of destructive interference of the scattered waves emanating from scatterers in different legs of the triskelion, being sensitively dependent upon the relative distance between the legs. The latter, in turn, is linked to the out-of-plane pucker of the triskelion. This feature in $I(q)$ seems to decrease slightly in amplitude as the molecular model is flattened, but the location of the dip in the $I(q)$ curve also changes. A noteworthy observation from the SANS data shown in Figs. 3 and 4 is that the dip, although predicted by calculations based on rigid, puckered triskelial models, does not exist as prominently in the experimental data. There it occurs only as a shoulder or plateau just outside the low q, Guinier regime, leading us to develop models based on flexibility (discussed below). A key point is that such smearing of the dip can be expected if the legs develop kinks.

Another interesting feature of the experimental SANS data is the power law decay of the scattered intensity noted for

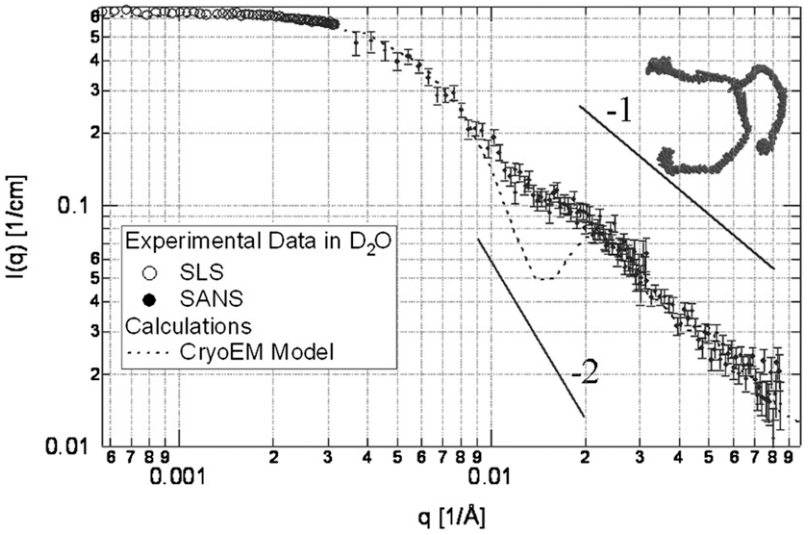

FIGURE 3 $I(q)$ determined by SLS (*open circles*) and SANS (*solid circles*) of clathrin triskelia in 0.5 M Tris/D_2O, compared with a calculated scattering curve based on a cryoEM structure of clathrin. SANS data are plotted on an absolute scale in units of cm^{-1}; the dashed line shows a scattering function calculated using Eq. 1 for a cryoEM structure of clathrin in a D_6 basket (shown in the *upper right-hand corner*), scaled by an empirically determined factor of 0.64 cm^{-1} so the calculated curve overlaps the SANS data in the range $0.0047\ Å^{-1} < q < 0.0075\ Å^{-1}$. (Note the concordance, also, between the data and the calculated curve at high q.) The light scattering data were scaled to fit the (adjusted) calculated curve over the range $0.0006\ Å^{-1} < q < 0.002\ Å^{-1}$. (The plotted SANS data reflect the fact that a measured background ($\approx$0.1 cm^{-1}), ascribed to the D_2O buffer, has been subtracted from SANS data; error bars are related to counting statistics.) The solid lines indicate the power laws q^{-2} (Eq. 3) and q^{-1} (Eq. 4), corresponding to the large q scaling of a flexible Gaussian chain model and a rigid rod, respectively.

large values of q. It falls off as $q^{-1.23}$ in D_2O, with the value of the exponent (-1.23) being somewhere between -1, corresponding to the behavior of a rigid rod model, and -2 for a random coil. This can be seen in Figs. 3 and 4, where the solid lines indicate the slopes (-1) and (-2).

Flexible models

The scattering cross section for a completely flexible model of a single linear chain polymer is given by Eq. 3. The form of that equation reflects interference scattering from the various monomers on the chain. By extension, the scattering cross section for a fully flexible molecule of three connected linear chains will show interference from scatterers in different chains, as well as from scatterers on the same chain. The scattering function falls off asymptotically as q^{-2} at large q, being described by the following equation (from Teraoka (24)):

$$I_3(q) = \frac{6}{R_g^4 q^4}\left(e^{-\frac{1}{3}R_g^2q^2}\left(e^{-\frac{1}{3}R_g^2q^2} - 1\right) + \frac{1}{3}R_g^2q^2\right). \qquad (5)$$

Thus, it is clearly seen that a fully flexible model for a clathrin triskelion will not fit SANS data at large values of q (see Supplementary Material, Data S1).

Smearing caused by a distribution of neutron wavelengths

In the NG3-SANS instrument, neutrons from the cold source pass through a multidisk mechanical velocity selector having

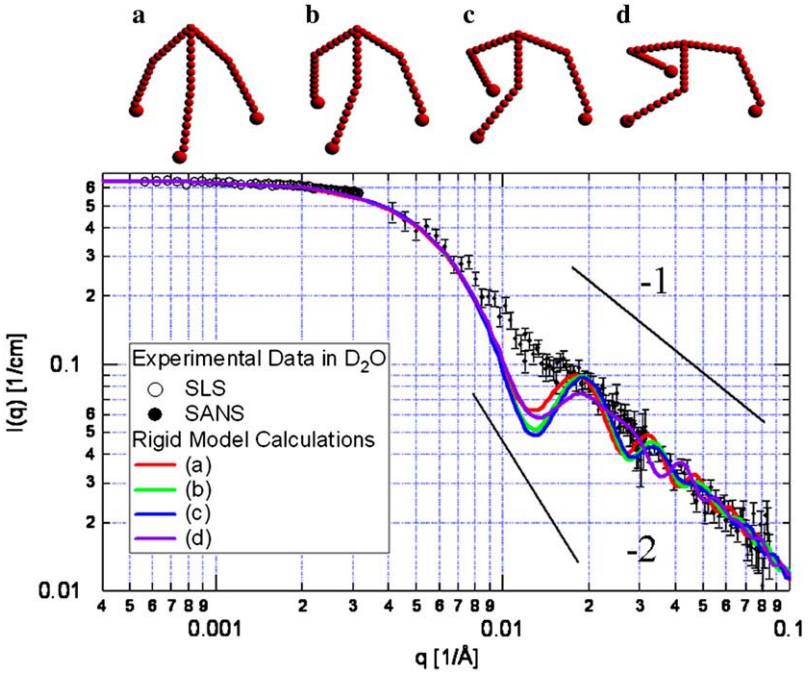

FIGURE 4 SLS data (*open circles*) and SANS data (*solid circles*) of clathrin in 0.5 M Tris/D_2O (see caption to Fig. 3), compared with calculated scattering curves for coarse-grained bead models of a rigid triskelion. The solid curves show scattering functions calculated using Eq. 1 for different models (*a–d*, *left* to *right* above figure) of a clathrin triskelion, which were made up of 52 beads (see text). These models are in agreement with previous light scattering measurements (SLS and DLS) of clathrin triskelia (4). As done for Fig. 3, the calculated scattering functions (which according to Eq. 1 tends to 1 at $q = 0$) were scaled by a factor of 0.64 cm^{-1}. Error bars on the data are related to counting statistics.

variable speed and pitch, enabling both the mean wavelength and wavelength resolution to be chosen. In our experiments the mean wavelength of the neutrons was 5.5 Å and the full width at half-maximum was 0.8 Å.

In the calculation of model scattering functions already presented, it was assumed that the incident and scattered wave vectors of interfering plane waves, $\vec{k}_0$ and $\vec{k}_s$, have a fixed magnitude. In practice, however, the incident neutron beam has a wavelength dispersion, which can be described with a Gaussian distribution function of the magnitude of the wavevector,

$$\rho(q) = \frac{1}{\sqrt{2\pi\sigma_q^2}} e^{-\frac{(q-q_0)^2}{2\sigma_q^2}},$$

where q_0 is the average wavevector and σ_q is related to the width of the distribution. Then, the actual scattering function will be an average of the diffraction patterns corresponding to multiple wavelengths, according to the following equation (25):

$$I_\rho(q|q_0,\sigma_q) = \int_0^\infty \rho(q')I(q')dq' = \frac{1}{\sqrt{2\pi\sigma_q^2}} \int_0^\infty I(q') e^{-\frac{(q-q_0)^2}{2\sigma_q^2}} dq'. \quad (6)$$

This transformation was applied to the triskelion model function for $q_0 = 5.5$ Å and $\sigma_q = 0.8$ Å . The results can be seen in Data S1. One finds from this calculation that smearing due to wavelength dispersion does not account for the disagreement between experiment and theory observed in Figs. 3 and 4.

Semiflexible models

Snapshots from a Brownian dynamics simulation of a bead-spring model of a clathrin triskelion were used to calculate a series of instantaneous scattering functions by Eq. 1. These functions were calculated and then averaged over time to produce an average scattering function which then could be compared with experimental measurements. Three such averaged scattering functions based on different triskelion flexibilities (as seen in differing values of persistence length, L_p) are shown in Fig. 5, along with the rigid-model cross section. We also show SLS and SANS data taken on clathrin triskelia in 0.5 M Tris/D_2O at pD* 7.0, and observe that curves of $I(q)$ calculated for the flexible models are in better agreement with experimental data, especially at intermediate q values. This shows that, while rigid models are appropriate for the calculation of average properties such as translational diffusion coefficients and the radius of gyration (4), additional information is included in the SANS scattering function that allows us to describe the molecular flexibility and dynamics of isolated triskelia.

As the rigidity of the bead-spring model is decreased, the dip and subsequent peak in the scattering cross section at intermediate q values are smoothed out, becoming only a shoulderlike feature. It should be noted that this shoulder occurs at the same value of q in which a shoulder is seen in the experimental data. However, in the extreme case that the flexibility is very large, even this feature disappears. Consequently, we conclude that very flexible models will not agree, even qualitatively, with the experimental SANS data. As previously mentioned, use of D_2O provides higher contrast between solute and solvent, allowing measurement of the scattering function at the higher values of q that are accessible with a detector distance of five meters. In Fig. 5, good agreement between SANS data and curves based on specific semiflexible models can be seen over the entire q range measured, which extends over two-and-a-half orders of magnitude. The curves shown in Fig. 5 *a* were calculated for structure appearing at the top of Fig. 4, but similar behavior is observed for structures in Fig. 5, *b–d*. Best agreement between calculations and data seems to be achieved when the persistence length of a triskelial leg is approximately one-half its length (see below).

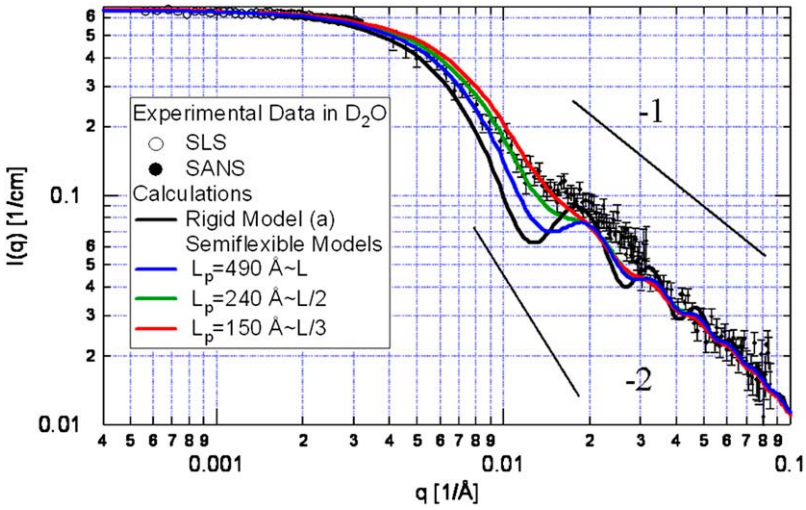

FIGURE 5 SLS data (*open circles*) and SANS data (*solid circles*) of clathrin in 0.5 M Tris/D_2O (see captions to Figs. 3 and 4), compared with calculated scattering functions of semiflexible models of a clathrin triskelion characterized by differing values of the persistence length, L_p. (Values are compared, in the *inset*, with clathrin leg length, *L*.) The lines show time-averaged scattering functions calculated from three flexible models of a clathrin triskelion based on the 52-bead model indicated as *a* at the top of Fig. 4. For comparison, we also show the cross section calculated for the corresponding rigid model. Error bars on the data are related to counting statistics.

Estimating model parameters from experimental measurements of clathrin triskelia

By fitting the SANS data with calculated curves of the proposed semiflexible model, one can estimate the persistence length of the individual triskelion. Here, we modeled a triskelion by a scheme similar to that used by Marques et al. (14) to approximate the motions of semiflexible linear polymers, as illustrated in Fig. 6. Briefly, the legs of the triskelion were represented by beads joined to each other with linear springs having a spring constant k representing forces between neighboring subunits. Other springs, linking next nearest-neighbors and having spring constant $k' = \alpha k$, were used to preserve bond angles. Torsional rotations at the hub were restricted by connections between the terminal domains of the legs (not shown), arbitrarily taken also to be springs having spring constant k. The leg length distribution (6) and the persistence length (26) of the legs of real clathrin triskelia have been estimated from the analysis of variations in electron micrographs of clathrin triskelia flattened on a mica surface. These estimates for the elasticity of a triskelion leg were used as first estimates of the model parameters, k and α, of our bead-spring model of a triskelion.

Brownian dynamics simulations were run for several different values of k and α at a temperature of 20°C for a total duration of 70 μs. Computation time varied with time step, which in turn was dependent upon the strongest spring in the simulation (αk) and the desired degree of accuracy ($\varepsilon = \frac{\alpha k \Delta t}{2\zeta} = 5\%$). Five-hundred snapshots of the configuration of each molecule were recorded during the simulation.

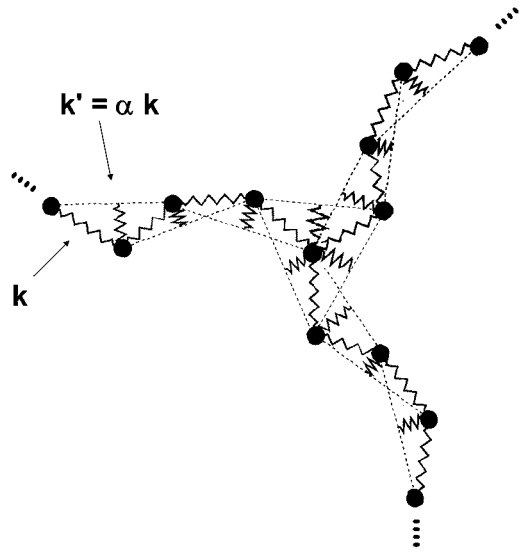

FIGURE 6 A schematic of the bead-spring model of a clathrin triskelion used in the Brownian dynamics simulation, showing the common hub and the first four subunits of each leg. Jagged lines represent springs between neighboring subunits, and dotted lines indicate springs between nonneighboring subunits. Torsional motion of the legs is partially prohibited by the addition of a single spring of strength k between each terminal domain (not shown). Some axial rotation is still unconstrained about the axis defined by the triskelion vertex and the end of the leg. Constraining this motion by the insertion of additional springs between the legs did not have a large affect on the time-averaged scattering functions. The figure is based on a scheme introduced in Marques et al. (14).

For a given set of spring strengths, k and $k' = (\alpha k)$, the leg extension flexibility of the bead-spring model was determined by the explicit calculation of temporal fluctuations in leg lengths during the simulation. Triskelial leg length fluctuations were dependent on the spring constants used, but were $<1\%$ of the total leg length for the parameter range that was simulated. Thus the model was effectively inextensible for the parameter ranges used in the simulation.

The persistence length of the triskelion legs, L_p, is dependent on the spring constants used in the simulation. L_p was determined explicitly from the simulation by calculating the spatial correlation function of the directional tangent vector cosine as a function of arc-length, s, with respect to a tangent vector defined between the vertex and the first subunit of each individual triskelion leg. Once calculated, the correlation functions were fit to an exponential curve with the decay length (the inverse slope of the straight line on a semilog plot) giving a measure of the persistence length, L_p (see Appendix and Data S1). In the simulations the persistence length was found to vary between 150 Å and 1000 Å for the range of model parameters studied. This can be compared with the experimentally estimated value of $L_p = 350$ Å which, as discussed in the Appendix, was determined by Jin and Nossal (26) from an analysis of electron micrographs.

The calculated persistence length of the simulation has been plotted in Fig. 7 as a function of spring strength, k, for different values of the model parameter α. The fitted curve (*dotted line*) suggests that the persistence length has an inverse square-root dependence on k. From the curve it is seen that the value of the persistence length estimated from electron micrographs (that is, 350 Å) corresponds, in this Brownian dynamics model, to a spring constant of $k \approx 180$ Da ps^{-2}. (The persistence length seems to be independent of α for the two values simulated, $\alpha = 10$ and $\alpha = 100$.) The curve in Fig. 5 that best fits the measured $I(q)$ is the one for $L_p = 240$ Å (spring constant, $k \approx 100$ Da ps^{-2}) which, considering the many approximations of our model, is remarkably close to the previously-determined value (26). It should be noted that the significant quantity, here, is the persistence length, rather than any particular parameter associated with a specific variant of the bead-spring model.

SUMMARY AND DISCUSSION

We previously used dynamic and static light scattering to assess the structural characteristics of clathrin triskelia in solution (4). In particular, we were able to rule out a rigid planar structure for the triskelion, demonstrating that the triskelia, on average, are puckered but less so than when they are incorporated into small, D_6 baskets. This qualitative result suggests that the triskelia change their shape as they insert

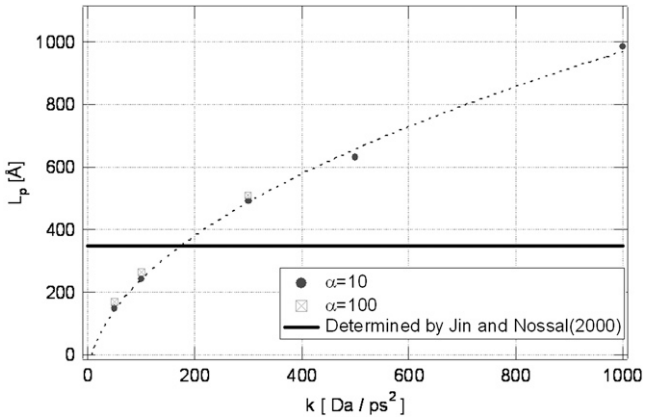

FIGURE 7 Dependence of the persistence length, L_p, upon the spring strength, k, as determined from a Brownian dynamics simulation of a bead-spring model performed at room temperature (see Appendix). Symbols show persistence lengths derived from the simulations, and the dotted line shows a square-root fit to the symbols for $\alpha = 10$. The dark solid line is drawn at the value of $L_p = 350$ Å previously determined by from electron micrographs (26).

into baskets of differing size, and that they also may change to accommodate their being in different locations within a basket. The light scattering measurements were interpretable in terms of a mean triskelial morphology, but there is insufficient information in such data to examine fluctuations about the average shape. The SANS measurements described in this article are consistent with the findings of the light scattering experiments of our earlier study, in that calculated curves for $I(q)$ fit SANS measurements at small values of q only when the triskelia are puckered. However there is additional information in the SANS cross sections at larger q that informs our understanding of triskelial structure. One immediately finds, for example, that a fully random, Gaussian chain model cannot adequately describe SANS measurements at large q (see Fig. 3).

It often is the case that SANS data are characterized in the form of a Kratky plot, i.e., $q^2I(q)$ versus q. Under certain circumstances, the slope of this curve provides useful information about the compactness of the target molecules (27). However, on the length scales of interest here, a triskelion is not compact; rather, it is a supramolecular structure having the shape—if collapsed on a planar surface—of a three-legged pinwheel (1,2), retaining such shape in three dimensions. The secondary structure of the clathrin heavy chain (the leg) is a coiled-coil (2), so unless the molecule is denatured its flexibility is likely to be somewhat limited. Indeed, this SANS study indicates that triskelia are semiflexible, in accordance with information about clathrin leg flexibility that was obtained by less direct methods (26,28).

The analysis presented in the earlier light scattering article was based on rigid models. These models also provide good fits to SANS measurements, except for a discrepancy at intermediate values of q. We have ruled out technical issues such as smearing of the data due to dispersion in neutron wavelengths as explanations for this disparity. Hence, we hypothesized that inconsistencies between the rigid puckered models and SANS measurements might be due to flexibility of the triskelions. Although it might be construed that the attenuated peak at $Q = 0.016$ Å^{-1} in the experimental SANS data indicates an ensemble of rigid triskelia trapped in different configurations, such interpretation would be at variance with our earlier study involving DLS (4), which indicated that the triskelion samples are essentially monodisperse. Moreover, the incorporation of rigid triskelia of fixed shape into growing baskets would have to be exquisitely orchestrated in order that triskelia with the correct configurations arrive at the polymerizing structures at just the right time. In this scenario the outcome of overall basket polymerization might be somewhat random, particularly if the initial triskelion concentration is low, since depletion of various species of rigid triskelia during the early instances of basket formation might affect the shapes of later-formed baskets. Slow annealing of baskets might occur, but the outcomes of reconstitution experiments could vary significantly, which appears not to be the case. More significantly, in studies performed on cell cultures of uniform type, coated vesicles holding different cargoes are found to have sizes that are linked with cargo identity (29), which is hard to reconcile with a trapped-conformation, rigid triskelion hypothesis. Finally, triskelia precipitated from solution onto mica surfaces show fluctuations in shape which are of approximately equal magnitude along the entire length of a leg (26) and, as pointed out above, demonstrate a persistence length that is similar to that derived in this SANS study.

The physical models that we use in our data analysis facilitate computations that would be difficult, if not impossible, to perform on much more detailed models. Our Brownian dynamics model clearly is based on a simplification of the actual macromolecular structure of a triskelion, and was used here primarily to obtain qualitative information about the effect of flexibility on the SANS cross section. To a certain degree, the main result concerning flexibility is model-independent, since the relevant descriptor for comparison with experiment is the persistence length. The consistency between the results of this investigation and those of our earlier studies (26) suggests that this approximate treatment has considerable merit. Secondarily, for the clathrin structure whose molecular coordinates are known with reasonable accuracy—namely, a triskelion in a D_6 basket—we find a clear discrepancy between the corresponding calculated SANS scattering cross section and the measured $I(q)$, reinforcing our earlier conclusion that flexibility needs to be taken into account to obtain quantitative understanding of how clathrin baskets assemble.

Thus we infer that isolated clathrin triskelia in solution have a puckered structure on average but may undergo significant shape changes due to thermal fluctuations, thereby facilitating clathrin basket assembly. However, triskelial flexibility probably is stabilized once a triskelion is posi-

tioned in a clathrin lattice. This might explain why basket structures can be determined by cryoEM tomography but the shapes of isolated, individual triskelia have not been resolved by this technique. If this indeed is the case, it would imply an entropic loss during clathrin lattice assembly, which may affect basket stability and thus be important in determining basket size distributions (30).

APPENDIX

Brownian dynamics simulations

To investigate the effects of thermal motions on $I(q)$, we constructed a discrete bead model of a triskelion and approximated intramolecular forces on each subunit by linear springs. A similar bead-spring model was proposed by Harris and Hearst (31) to approximate semiflexible linear polymers and later studied by Marques et al. (14). In those models, bonds between molecular subunits have identical spring constants and bond angles are preserved by springs of a different strength between next-nearest neighbors. Unlike the wormlike chain model of Kratky and Porod (25), which uses a fixed bond length, the Harris and Hearst model allows for bond-length fluctuations determined by the strength of the springs and the temperature of the reservoir. In our model, equilibrium bond lengths are determined from a structural model and bond-length fluctuations are suppressed by the use of stiff springs (see Fig. 6). The model preserves bond lengths and bond angles, while allowing flexibility of the triskelion legs. Bead size and equilibrium configurations were chosen according to the models described in Ferguson et al. (4), which were based on structural and light scattering measurements of clathrin triskelia.

We simulated dynamics of the triskelion model in a thermal bath by integrating a Langevin equation (32) of the form

$$m_{\mathrm{i}}\frac{d^2x_{\mathrm{i}}}{dt^2} = F_{\mathrm{i}}(t) + \mathcal{F}_{\mathrm{i}}(t), \tag{7}$$

where m_{i} is the mass of a subunit i, x_{i} is the subunit position (in one dimension), $F_{\mathrm{i}}(t)$ is the total intramolecular force on a subunit i at time t, and $\mathcal{F}_{\mathrm{i}}(t)$ is the random thermal force on the subunit from the surrounding fluid. The latter may be split into a slowly varying frictional force proportional to the velocity of the subunit, $-\zeta_1(dx_{\mathrm{i}}/dt)$, and a rapidly varying force, $F_{\mathrm{i}}'(t)$, that averages to zero. Equation 7 thus may be written as

$$m_{\mathrm{i}}\frac{d^2x_{\mathrm{i}}}{dt^2} = F_{\mathrm{i}}(t) - \zeta_{\mathrm{i}}\frac{dx_{\mathrm{i}}}{dt} + F_{\mathrm{i}}'(t);\ \langle F_{\mathrm{i}}'(t)\rangle = 0, \tag{8}$$

where ζ_{i} is the friction constant of a single subunit i, here approximated by Stokes' law $\zeta_{\mathrm{i}} = 6\pi\eta a_{\mathrm{i}}$, where η is the viscosity of the surrounding fluid ($\eta_{\mathrm{Water}} = 0.001\ \mathrm{Pas} = 60.2\,\frac{\mathrm{Da}}{\mathrm{\AA\,ps}}$) and a_{i} is the radius of the spherical subunit (33).

New coordinates for each subunit of our molecule are determined by a simple Eulerian integration of Eq. 8 since the inertial term, $m_{\mathrm{i}}(d^2x_{\mathrm{i}}/dt^2)$, is small and can be ignored (34), i.e.,

$$x_{\mathrm{n}+1} = x_{\mathrm{n}} + \frac{\Delta t}{\zeta}F(\{x_{\mathrm{n}}\}) + X_{\mathrm{n}}, \tag{9}$$

where x_{n} is the subunit position at step n (the particle index, i, has been suppressed here) and $F(\{x_{\mathrm{n}}\})$ is the total intramolecular force on a subunit at time step n. Δt is the time step and X_{n} is a random displacement simulating thermal collisions with solvent molecules, having the properties $\langle X_{\mathrm{n}}\rangle = 0$ and $\langle X_{\mathrm{n}}^2\rangle = 2D_{\mathrm{i}}\Delta t$, where $D_{\mathrm{i}} = (k_{\mathrm{B}}T/\zeta_{\mathrm{i}})$ is the diffusion coefficient of the subunit i in the absence of other subunits.

The numerical integration of Eq. 8 has an error associated with it that is dependent upon the time step Δt used in Eq. 9. We can evaluate this error for the simple case of a particle in a harmonic potential of strength k (the primary spring constant between beads—see Fig. 5) and a thermal reservoir at temperature T (33) so that the mean-squared displacement $\langle x^2\rangle$ is given by $(k_{\mathrm{B}}T/k)$. By squaring Eq. 9, substituting $F = -kx_{\mathrm{n}}$, taking the time average (denoted by $\langle\ldots\rangle$), and assuming that $\langle x_{\mathrm{n}+1}^2\rangle = \langle x_{\mathrm{n}}^2\rangle$ and $\langle x_{\mathrm{n}}X_{\mathrm{n}}\rangle = 0$, we find

$$\langle x_{\mathrm{n}}^2\rangle = \frac{k_{\mathrm{B}}T}{k}\frac{1}{1-\varepsilon};\ \varepsilon = \frac{k\Delta t}{2\zeta}. \tag{10}$$

The time step, Δt, was chosen such that the numerical error, ε, in $\langle(x_{\mathrm{n}}^2)\rangle$ of the strongest spring used in the simulation, k, was 5%, or explicitly that $\Delta t = \frac{1}{10}\frac{\zeta}{k}$.

Constructing a bead-spring model of a triskelion

The mass of each subunit, $m_{\mathrm{i}} = \frac{4\pi}{3}\rho a_{\mathrm{i}}^3$, was calculated using the density of $\rho = 1.38$ g/mL (0.831 Da/Å^3), consistent with experimental measurements of other proteins (35). The radius of a subunit from the model was $a_{\mathrm{i}} = 15$ Å for legs and 25 Å for terminal domains. The mass of each subunit of the legs was ~12 kDa and the mass of each terminal domain was 54 kDa. This approximated the known molecular weight of a clathrin triskelion ($M_{\mathrm{w}} \sim$ 651 kDa) to within 13%. The three-dimensional intramolecular force on each subunit, $\vec{F}_{\mathrm{i}}(t)$ was approximated by springs of strength k between two neighboring subunits and springs of strength αk between two next-nearest neighboring subunit (see Fig. 6, above). Each bead in the leg of a triskelion had, on average, four springs connected to it. Each terminal subunit, where there is only one next-nearest neighbor, had two. The vertex, where there were three nearest neighbors and three next-nearest neighbors, was connected to other subunits by six springs. This constrained the angles between each leg at the vertex. To constrain the legs of the triskelion from twisting, each of the terminal subunits was connected by a spring of strength k (identical to the strength of springs between neighboring subunits in the legs). Thus, $\vec{F}_{\mathrm{i}}(t)$ is a function of the coordinates of neighboring subunits and for typical subunits can be written explicitly as

$$\begin{aligned}\vec{F}_{\mathrm{i}}(t) = {}& \alpha k(\vec{x}_{\mathrm{i}-2}(t) - \vec{x}_{\mathrm{i}}(t) - \vec{x}_{\mathrm{i}-2}(0) + \vec{x}_{\mathrm{i}}(0))\\ &+ k(\vec{x}_{\mathrm{i}-1}(t) - \vec{x}_{\mathrm{i}}(t) - \vec{x}_{\mathrm{i}-1}(0) + \vec{x}_{\mathrm{i}}(0))\\ &+ k(\vec{x}_{\mathrm{i}+1}(t) - \vec{x}_{\mathrm{i}}(t) - \vec{x}_{\mathrm{i}+1}(0) + \vec{x}_{\mathrm{i}}(0))\\ &+ \alpha k(\vec{x}_{\mathrm{i}+2}(t) - \vec{x}_{\mathrm{i}}(t) - \vec{x}_{\mathrm{i}+2}(0) + \vec{x}_{\mathrm{i}}(0)).\end{aligned} \tag{11}$$

The initial position of each subunit, $\vec{x}_{\mathrm{i}}(0)$, was chosen from the equilibrium model (a) shown at the top of Fig. 4. This model and the other three appearing in Fig. 4 have values of hydrodynamic radius, r_{H}, and radius of gyration, r_{g}, very close to those measured by light scattering experiments performed on clathrin triskelia in solution (4). Results of the analysis described here are qualitatively similar when the other models are examined.

The bending rigidity has been estimated from an experimental distribution of triskelions

Fluctuations in the shape of a linear filament can be characterized by the persistence length, L_{p}, which is a measure of the flexibility of a filament. L_{p} can be determined experimentally from the spatial correlation function of the tangent vector, $\hat{\theta}(s)$, where s is the arc-length measured along the filament. The spatial correlation function of the cosine between two tangent vectors, $\hat{\theta}(0)$ and $\hat{\theta}(s)$, at a distance s from each other along the filament decays exponentially in three dimensions according to

$$\langle\hat{\theta}(s)\cdot\hat{\theta}(0)\rangle = e_{\mathrm{p}}^{-\mathrm{s/L}}, \tag{12}$$

where $\langle\ldots\rangle$ denotes a time or ensemble average.

In a continuous elastic medium of Young's modulus, E, and cross-sectional second moment, $I = \int r^2 dA$, the persistence length of an elastic filament can be related to the flexural rigidity, EI, through the equipartition

theorem. In two dimensions, the energy stored in the deformation of an elastic filament of length L and flexural rigidity EI is given by

$$U = \frac{1}{2} EI \sum_{n=1}^{\infty} \left(\frac{n\pi}{L}\right)^2 (a_n - a_n^0)^2,$$

where a_n^0 is the amplitude of the n^{th} Fourier mode of the shape descriptor in the absence of forces and a_n is the amplitude when the filament is distorted (26,36,37). Since in equilibrium the average energy stored in a Fourier mode is 1/2 $k_B T$, the flexural rigidity can be related to the persistence length, L_p, by

$$L_p = \frac{EI}{k_B T}. \tag{13}$$

When the shape fluctuations in electron micrographs of triskelion legs were analyzed this way (26), the flexural rigidity of a triskelion leg was estimated to be $EI = 350\, k_B T$ Å from the first five Fourier modes, giving triskelion legs a persistence length of 350 Å or $(L_p/\langle L\rangle) = (350\,\text{Å}/516\,\text{Å}) \sim (2/3)$, where $\langle L\rangle$ is the average length of a triskelial leg.

In the simulations described in the main part of this article, we showed how the scattering cross section varies with different values of the model parameters k and α (see Fig. 5). The simulations also yield a value of the persistence length according to Eq. 12 (see, also, Data S1), which can be compared with the value determined from electron microscopy (as is done in Fig. 7, above).

Computation of time averages from dynamic simulations

To determine how long to run the simulation for computation of a meaningful time average of dynamic quantities, the timescales related to internal modes of oscillation of the bead-spring model need to be estimated. Since we are interested in computing a time-averaged scattering function, we will concentrate on fluctuations in the radius of gyration, r_g, which is loosely related to the width of the central peak in the scattering function. The radius of gyration can be defined as the second moment of the mass distribution, $\rho(\vec{x})$, in a molecule as $r_g = \int_V d\vec{x}|\vec{x}|^2\rho(\vec{x})$. When the molecule is modeled as a discrete set of spherical subunits, where $\vec{x}_i$ is a subunit position with respect to the center of mass, a_i is the subunit radius, and $v_i = \frac{4\pi}{3}a_i^3$ is a subunit volume, r_g is given by

$$r_g = \frac{1}{N}\frac{\sum_{i=1}^{N} v_i|\vec{x}_i|^2}{\sum_{i=1}^{N} v_i}.$$

In general, during simulations this quantity is time-dependent, i.e., $r_g(t) = r_g(\{\vec{x}_i(t), a_i\})$, so the radius of gyration of the bead-spring triskelion model can be considered a dynamic variable and is a function of the bead coordinates and radii. The temporal autocorrelation function of the instantaneous radius of gyration can tell us something about the timescales with which the model conformation, and therefore the scattering function, is fluctuating.

In the Brownian dynamics simulation, r_g is found to fluctuate about an average value that is 5–18% below the value of the rigid model, r_{g0}, and approaches that value, as the spring strength is increased to the rigid model limit. The root-mean square fluctuation in the r_g value is ~10 Å and is a weak function of spring strengths, k, and αk. When we calculated the temporal autocorrelation function $\delta r_g = r_g(t) - \langle r_g\rangle$ by the equation

$$\frac{\langle \delta r_g(\tau)\delta r_g(0)\rangle}{\langle \delta r_g^2\rangle} = \frac{\frac{1}{T}\int_0^T \delta r_g(t+\tau)\delta r_g(t)dt}{\frac{1}{T}\int_0^T \delta r_g(t)^2 dt} \sim e^{-\tau/\tau_c},$$

we noted that it had an initial, rapid exponential decay in delay time, τ_C, between 0.5 and 1.3 μs, for different spring strengths, k.

SUPPLEMENTARY MATERIAL

To view all of the supplemental files associated with this article, visit www.biophysj.org.

This work was supported in part by extramural National Institutes of Health grant No. NS29051 (to E.M.L.) and by intramural funds from the Eunice Kennedy Shriver National Institute of Child Health and Human Development. We utilized facilities at the NIST Center for Neutron Research that are supported in part by the National Science Foundation under agreement No. DMR-0454672.

REFERENCES

1. Kirchhausen, T. 2000. Clathrin. *Annu. Rev. Biochem.* 69:699–727.
2. Brodsky, F. M., C. Y. Chen, C. Knuehl, M. C. Towler, and D. E. Wakeham. 2001. Biological basket weaving: formation and function of clathrin-coated vesicles. *Annu. Rev. Cell Dev. Biol.* 17:517–568.
3. Stagg, S. M., P. LaPointe, and W. E. Balch. 2007. Structural design of cage and coat scaffolds that direct membrane traffic. *Curr. Opin. Struct. Biol.* 17:221–228.
4. Ferguson, M. L., K. Prasad, D. L. Sackett, H. Boukari, E. M. Lafer, and R. Nossal. 2006. The conformation of a clathrin triskelion in solution. *Biochemistry.* 45:5916–5922.
5. Fotin, A., Y. F. Cheng, P. Sliz, N. Grigorieff, S. C. Harrison, T. Kirchhausen, and T. Walz. 2004. Molecular model for a complete clathrin lattice from electron cryomicroscopy. *Nature.* 432:573–579.
6. Wakeham, D. E., J. A. Ybe, F. M. Brodsky, and P. K. Hwang. 2000. Molecular structures of proteins involved in vesicle coat formation. *Traffic.* 1:393–398.
7. Kocsis, E., B. L. Trus, C. J. Steer, M. E. Bisher, and A. C. Steven. 1991. Image averaging of flexible fibrous macromolecules—the clathrin triskelion has an elastic proximal segment. *J. Struct. Biol.* 107:6–14.
8. Musacchio, A., C. J. Smith, A. M. Roseman, S. C. Harrison, T. Kirchhausen, and B. M. Pearse. 1999. Functional organization of clathrin in coats: combining electron cryomicroscopy and x-ray crystallography. *Mol. Cell.* 3:761–770.
9. Sackett, D. L., V. Chernomordik, S. Krueger, and R. Nossal. 2003. Use of small-angle neutron scattering to study tubulin polymers. *Biomacromolecules.* 4:461–467.
10. Norman, A. I., R. Ivkov, J. G. Forbes, and S. C. Greer. 2005. The polymerization of actin: structural changes from small-angle neutron scattering. *J. Chem. Phys.* 123:154904.
11. Debye, P. 1944. Light scattering in solutions. *J. Appl. Phys.* 15:338–342.
12. Zimm, B. H., R. S. Stein, and P. Doty. 1945. Classical theory of light scattering from solutions—a review. *Polym. Bull.* 1:90–119.
13. McIntyre, D., and F. Gornick. 1964. Light Scattering from Dilute Polymer Solutions. Gordon and Breach, New York.
14. Marques, C. M., and G. H. Fredrickson. 1997. Rigid Gaussian chains I: The scattering function. *J. Phys. II France.* 7:1805–1816.
15. Morgan, J. R., K. Prasad, W. Hao, G. J. Augustine, and E. M. Lafer. 2000. A conserved clathrin assembly motif essential for synaptic vesicle endocytosis. *J. Neurosci.* 20:8667–8676.
16. Glasoe, P. K., and F. A. Long. 1960. Use of glass electrodes to measure acidities in deuterium oxide. *J. Phys. Chem.* 64:188–190.
17. Glinka, C. J., J. G. Barker, B. Hammouda, S. Krueger, J. J. Moyer, and W. J. Orts. 1998. The 30 m small-angle neutron scattering instruments at the National Institute of Standards and Technology. *J. Appl. Cryst.* 31:430–445.
18. Kline, S. 2006. Reduction and analysis of SANS and USANS data using IGOR Pro. *J. Appl. Cryst.* 39:895–900.

19. Naranjan, P. S., P. B. Yim, J. G. Forbes, S. C. Greer, J. Dudowicz, K. F. Freed, and J. F. Douglas. 2003. The polymerization of actin: thermodynamics near the polymerization line. *J. Chem. Phys.* 119:4070–4084.

20. Hardy, R. C., and R. L. Cottington. 1949. Viscosity of deuterium oxide and water from 5° to 125° C. *J. Chem. Phys.* 17:509–510.

21. Cho, C. H., J. Urquidi, S. Sing, and G. W. Robinson. 1999. Thermal offset viscosities of liquid H_2O, D_2O, and T_2O. *J. Phys. Chem. B.* 103:1991–1994.

22. Tirado Garcia, M. M., M. A. Jimenez Rios, and J. M. Garcia Bernal. 1990. Translational diffusion and intrinsic viscosity of globular proteins. Theoretical predictions using hydrated hydrodynamic models. Application to BPTI. *Int. J. Biol. Macromol.* 12:19–24.

23. Hellweg, T., W. Eimer, E. Krahn, K. Schneider, and A. Muller. 1997. Hydrodynamic properties of nitrogens: the MoFe protein from *Azobacter vinelandii* studied by dynamic light scattering and hydrodynamic modeling. *Biochim. Biophys. Acta.* 1337:311–318.

24. Teraoka, I. 2002. Polymer Solutions: An Introduction to Physical Properties. Wiley-Interscience, Brooklyn, NY.

25. Glatter, O., and O. Kratky. 1982. Small Angle X-Ray Scattering. Academic Press, New York.

26. Jin, A. J., and R. Nossal. 2000. Rigidity of triskelion arms and clathrin nets. *Biophys. J.* 78:1183–1194.

27. Calmettes, P., D. Durand, M. Desmadril, P. Minard, V. Receveur, and J. C. Smith. 1994. How random is a highly denatured protein? *Biophys. Chem.* 53:105–114.

28. Nossal, R. 2005. Mechanical aspects of clathrin cage formation. *Macromol. Symp.* 227:17–26.

29. Ehrlich, M., W. Boll, A. Van Oijen, B. Hariharan, K. Chandran, M. L. Nibert, and T. Kirchhausen. 2004. Endocytosis by random initiation and stabilization of clathrin-coated pits. *Cell.* 118:591–605.

30. Nossal, R. 2001. Energetics of clathrin basket assembly. *Traffic.* 2:138–147.

31. Harris, R. A., and J. E. Hearst. 1966. On polymer dynamics. *J. Chem. Phys.* 44:2595–2602.

32. Reif, F. 1964. Fundamentals of Statistical and Thermal Physics. McGraw-Hill, New York.

33. Pastor, R. W. 1994. Techniques and applications of Langevin dynamic simulations. *In* The Molecular Dynamics of Liquid Crystals. G. R. Luckhurst and C. A. Veracini, editors. Kluwer Academic Publishers. Amsterdam, The Netherlands.

34. Pastor, R. W., and M. Karplus. 1988. Parameterization of the friction constant for stochastic simulations of polymers. *J. Phys. Chem.* 92:2636–2641.

35. Fischer, H., I. Polikarpov, and A. F. Craievich. 2004. Average protein density is a molecular-weight-dependent function. *Protein Sci.* 13:2825–2828.

36. Gittes, F., B. Mickey, J. Nettleton, and J. Howard. 1993. Flexural rigidity of microtubules and actin filaments measured from thermal fluctuations in shape. *J. Cell Biol.* 120:923–934.

37. Howard, J. 2001. Mechanics of Motor Proteins and the Cytoskeleton. Sinauer Associates, Sunderland, MA.